Evolution of Nanowire Transmon Qubits and Their Coherence in a Magnetic Field

F. Luthi,[1,2] T. Stavenga,[1,2] O. W. Enzing,[1,2] A. Bruno,[1,2] C. Dickel,[1,2] N. K. Langford,[1,2] M. A. Rol,[1,2]
T. S. Jespersen,[3] J. Nygård,[3,4] P. Krogstrup,[3] and L. DiCarlo[1,2,*]
[1]*QuTech, Delft University of Technology, Lorentzweg 1, 2628 CJ Delft, Netherlands*
[2]*Kavli Institute of Nanoscience, Delft University of Technology, Lorentzweg 1, 2628 CJ Delft, Netherlands*
[3]*Center for Quantum Devices, Niels Bohr Institute, University of Copenhagen, DK-2100 Copenhagen, Denmark*
[4]*Nano-Science Center, Niels Bohr Institute, University of Copenhagen, DK-2100 Copenhagen, Denmark*

(Received 22 November 2017; published 9 March 2018)

We present an experimental study of flux- and gate-tunable nanowire transmons with state-of-the-art relaxation time allowing quantitative extraction of flux and charge noise coupling to the Josephson energy. We evidence coherence sweet spots for charge, tuned by voltage on a proximal side gate, where first order sensitivity to switching two-level systems and background $1/f$ noise is minimized. Next, we investigate the evolution of a nanowire transmon in a parallel magnetic field up to 70 mT, the upper bound set by the closing of the induced gap. Several features observed in the field dependence of qubit energy relaxation and dephasing times are not fully understood. Using nanowires with a thinner, partially covering Al shell will enable operation of these circuits up to 0.5 T, a regime relevant for topological quantum computation and other applications.

DOI: 10.1103/PhysRevLett.120.100502

Circuit quantum electrodynamics (CQED) offers unprecedented control over coupled atomic and photonic degrees of freedom in engineerable, microscale superconducting circuits [1,2]. It crucially relies on the dissipationless nonlinearity of the Josephson effect between two weakly coupled superconductors [3]. The Josephson junction (JJ), usually implemented as a superconductor-insulator-superconductor (SIS) tunnel barrier, allows the realization of anharmonic oscillators that can be operated in the quantum regime and used as qubits [4]. Circuit QED has found applications in many areas, including scalable quantum computation [5], quantum optics [6], quantum foundations [7], and quantum measurement and control [8]. So far, CQED has been limited by standard SIS JJs based on aluminum and its oxide to fields <10 mT, the critical field of bulk aluminum [9]. However, interesting applications such as coupling CQED devices to polarized electron-spin ensembles serving as quantum memories [10] and using qubits as charge-parity detectors in Majorana based topological quantum computation [11,12] require fields of $\sim$0.5 T. In such fields, more fundamental effects, such as topological phase transitions [13] and degeneracy lifting of the Andreev bound states which underlie the Josephson effect [14–17], can be studied. Entering this important regime for CQED requires the use of field-compatible superconductors and nonstandard JJs [18–22].

To date, qubits in CQED architectures have been realized using various JJs: the ubiquitous SIS tunnel junction [4], atomic break junctions [23], and semiconductor weak-link nanowire junctions [24–26]. Nanowire qubits are of particular interest because of potential compatibility with high magnetic fields, the voltage tunability of the JJ, and the overlap with other technologies of interest, including nanowire-based transistors and lasers [27,28]. Nanowire qubits are compatible with the transmon geometry [29], the most widely used in CQED, and have been realized in flux and voltage tunable variants [24,25]. Nanowire transmons have reached echo dephasing times (T_2^{Echo}) up to 10 μs, and been used to implement two-qubit gates [26]. So far, the use of Al as a superconductor for the larger scale CQED elements [25,26] and short coherence times [24] have inhibited study of the coherence of these circuits in a magnetic field.

In this Letter, we present an experimental study of decoherence processes affecting flux- and gate-tunable transmons based on nanowire Al-InAs-Al junctions, both at zero and applied magnetic fields. As is typical for conventional transmons, we observe the coupling of flux noise to the Josephson energy in a split-junction device. We estimate the flux noise spectrum from measurements of qubit dephasing with respect to flux sensitivity. Crucially, taking advantage of a state-of-the-art qubit relaxation time, we can also observe the coupling of charge noise directly to the Josephson energy. This noise takes the form of switching two-level systems and a $1/f$ background. Tuning the voltage side gate, we demonstrate coherence sweet spots at points where the first-order qubit sensitivity to charge is minimized. Paralleling the method used to study flux noise, we measure qubit dephasing as a function of this sensitivity to extract properties of the charge noise spectrum. Finally, we investigate the evolution of the qubit relaxation and dephasing as a function of the in-plane magnetic field, up to

the closing of the induced superconducting gap at 70 mT. Several features of the field dependence are not understood, calling for further experimental and theoretical investigation.

Device fabrication combines widely used NbTiN-based recipes for microscale features [30–32] with nanowire etching and contacting recipes. The nanowires have an InAs core and an epitaxially grown Al shell that induces a hard superconducting gap [20,33–37]. A home-made image recognition software defines etch and contacting masks [38–43] of the individual wires. After defining the superconductor-semiconductor-superconductor (SNS) junction by wet-etching a 200 nm segment of the 30 nm thick shell, the wires are contacted with NbTiN. Standard CQED control and measurement schemes [1,44–46] are used to probe the qubits that are coupled to the common feed line via dedicated readout resonators [47].

Following previous work [24], first, we extract information about the SNS junctions by studying the spectrum of the flux-tunable, split-junction device. A current I in the flux-bias line changes the magnetic flux Φ through the superconducting quantum interference device (SQUID) loop [Fig. 1(a)], controlling the superconducting phase difference $\hat{\delta}$ between the transmon islands. This tunes E_J, given in the short-junction, single-channel limit by Andreev bound states with transmission probability T_i and energy $V_i(\phi_i) = -\Delta_i\sqrt{1 - T_i \sin^2(\phi_i/2)}$. Employing the bound-state model in the split-junction Cooper-pair-box Hamiltonian, $\hat{H} = 4E_C\hat{N}^2 + V_A(\hat{\delta}) + V_B(2\pi\Phi/\Phi_0 - \hat{\delta})$, yields good agreement with the observed spectrum [Fig. 1(b)] [24]. The best-fit values of the induced gaps $\Delta_A/h = 46 \pm 4$ GHz and $\Delta_B/h = 38.5 \pm 0.9$ GHz are close to the 43 GHz of bulk Al, suggesting that the shell fully proximitizes the nanowire [35].

We investigate the flux noise of the split-junction qubit by measuring coherence times as a function of flux offset. T_2^{Echo} is T_1 limited in a range around ~20 MHz around the flux sweet spot [Fig. 1(c)]. The noise is quantified [38,48–50] using a second-order polynomial fit of the echo dephasing rate $\Gamma_\varphi^{\mathrm{Echo}} = 1/T_\varphi^{\mathrm{Echo}} = 1/T_2^{\mathrm{Echo}} - 1/(2T_1)$ versus $|\partial f_{01}/\partial\Phi|$. We extract a white-noise contribution to the double-sided spectral density $S_{\Phi,\mathrm{white}} = (60\mathrm{n}\Phi_0/\sqrt{\mathrm{Hz}})^2$ (from the quadratic term), a $1/f$ noise amplitude $\sqrt{A_\Phi} = 13.0\mu\Phi_0$ where $S_{\Phi,1/\mathrm{f}} = A_\Phi/|f|$ (from the linear term), and a 2 ms^{-1} offset. This value of $\sqrt{A_\Phi}$ is on the high side of the range observed for flux-tunable SIS transmons [49–52]. White flux noise has not been reported in these more standard systems.

Ramsey measurements reveal a beating pattern of two exponentially decaying sinusoids [Fig. 2(a)], indicating a switching of the qubit frequency f_{01} between two values. This is the reason for not reporting Ramsey coherence times (T_2^*) in Fig. 1. The observed frequency difference $\Delta f = f_{01}^{\mathrm{A}} - f_{01}^{\mathrm{B}} = 1.6$ MHz is nearly constant overnight [Fig. 2(b)]. Because Δf is constant and much larger than

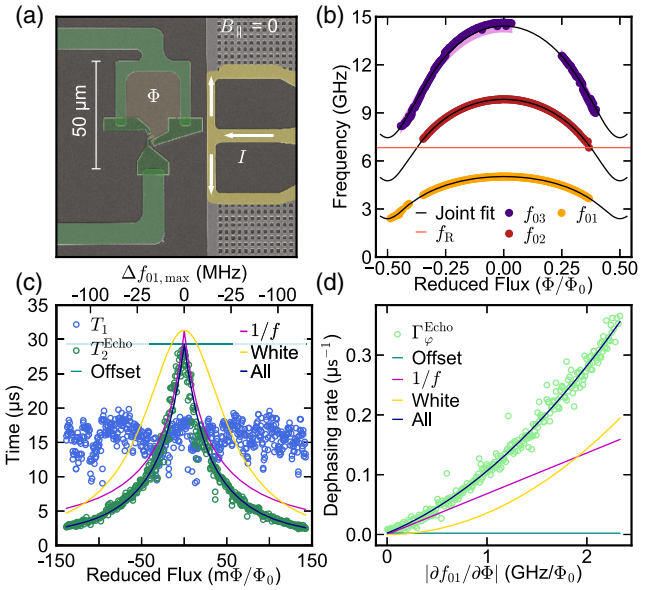

FIG. 1. Characterization of flux-tunable split-junction qubit at $B_\parallel = 0$. (a) False-colored SEM micrograph of the SQUID-loop area. The current I in the flux-bias line (yellow) threads a magnetic flux Φ through the SQUID loop (green), tuning $E_J(\Phi)$. (b) The joint fit (black) of the first three transitions (orange, dark red, and purple symbols) versus flux yields the transmission probability and the induced gap of each junction. (c) T_1 (blue symbols) limits T_2^{Echo} (green symbols) at the qubit flux sweet spot $\Phi = 0$. A fit to T_2^{Echo} that includes the measured T_1 limit allows extraction of flux-independent (cyan line), $1/f$ (pink line) and white-noise (gold line) contributions to the dephasing. T_2^* is typically below 4 μs. Top axis indicates the frequency detuning from the flux sweet spot. (d) $\Gamma_\varphi^{\mathrm{Echo}}$ versus flux sensitivity, extracted from (c), with the different contributions to the fit.

the calculated charge dispersion [29] of 200 kHz, we conclude that the switching is due to a two-level systems (TLS) coupling directly to the nanowire E_J. Furthermore, we attribute the correlated jumps in the two frequencies to other TLSs switching on slower time scales. Using the qubit, we monitor the fast TLS in real time using a single-shot Ramsey-based pulse sequence tailored for Δf [Fig. 2(c)] [53]. The double-sided power spectral density (PSD) of the TLS state time evolution is well explained by an asymmetric random telegraph noise (RTN) with characteristic switching times of 100 ms [Fig. 2(d)] [38]. Better agreement with the measured PSD is achieved by taking $1/f$ noise into account [38]. The switching of f_{01} between multiple values can be observed in several qubits. In addition, the Δf of gatemons was observed to depend on V_G [38]. This dependence indicates that the TLSs are charge traps in the vicinity of the junction, influencing the transmission probabilities of the Andreev bound states.

Now, we study the spectrum of a gatemon as a function of V_G [Figs. 3(a)–3(d)]. Tuning V_G changes f_{01} by altering the T_i, hence, altering E_J. The anharmonicity $\alpha = f_{02} - 2f_{01}$ (f_{02} is the transition from the ground to the

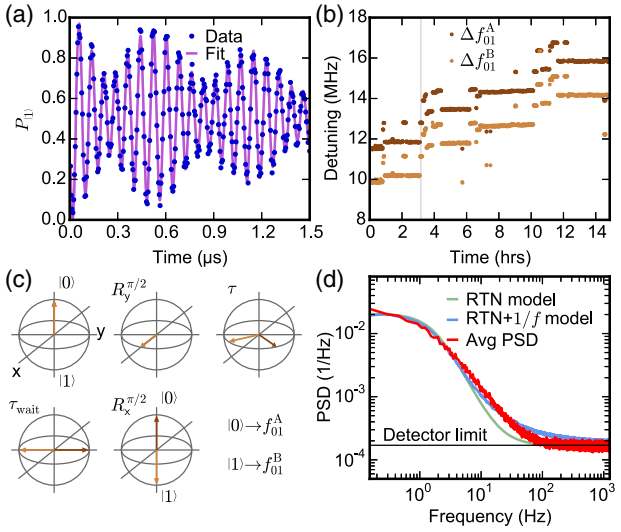

FIG. 2. Frequency stability analysis of the flux-tunable qubit at the flux sweet spot and at $B_\parallel = 0$. (a) Ramsey experiment (dots) with artificial detuning (12 MHz). The strongly coupled TLS yields a beating between two decaying sinusoids (purple line, $\tau^{\mathrm{A}} = 2.2\ \mu$s, and $\tau^{\mathrm{B}} = 2.0\ \mu$s). (b) The extracted detunings of repeated Ramsey experiments show a constant frequency spacing and drift of the center frequency. The gray vertical line indicates the trace in (a). (c) Pulse sequence of the Ramsey-type TLS-state detection scheme. The free evolution time τ is chosen as $\tau_{\mathrm{wait}} = 1/2\Delta f$ for maximal contrast. (d) The PSD (red line) of the TLS is computed from qubit state traces obtained by monitoring the qubit frequency real time using the pulse sequence in (c). The PSD is fitted using RTN models with (blue line) and without (green line) $1/f$ noise.

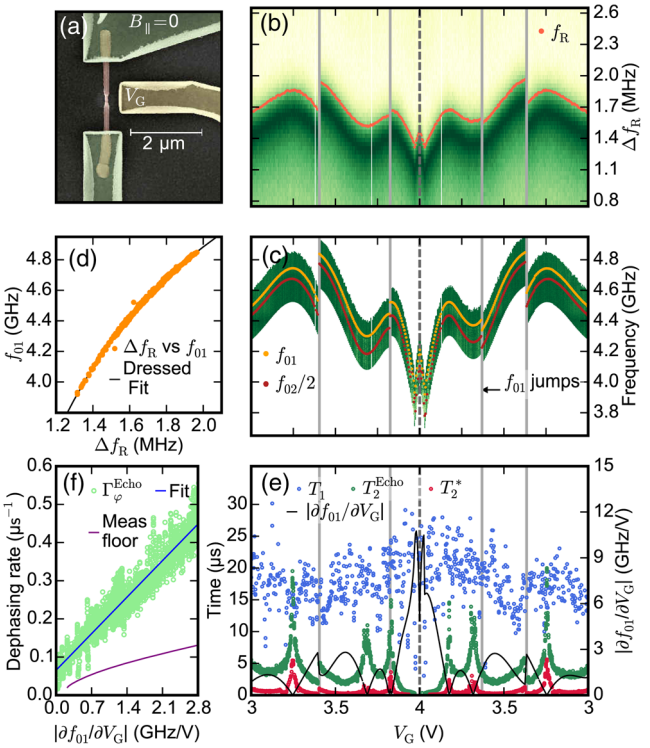

FIG. 3. Gatemon characterization at $B_\parallel = 0$. (a) False-colored SEM micrograph of the nanowire Josephson junction (light red) with a side gate (yellow) enabling V_G tuning. (b) Deviation of f_R, Δf_R, from the bare resonator frequency $f_{\mathrm{bare}} = 6.732$ GHz for a triangle sweep in V_G. Note the change in direction of the V_G sweep, indicated by the dashed line. On return to the same V_G, f_R is roughly reproduced. (c) f_{01} versus V_G. Random, but sometimes reproducible jumps of f_{01} occur (at light gray lines). (d) Plot of f_{01} against f_R (orange dots) and dressed state fit (black curve) with coupling strength $g/2\pi = 60.8$ MHz, allowing a prediction of f_{01}. (e) Gatemon T_1 (blue symbols), T_2^{Echo} (green symbols), and T_2^* (red symbols) versus V_G. Both T_2^{Echo} and T_2^* are strongly correlated with the V_G sensitivity (black line). (f) $\Gamma_\varphi^{\mathrm{Echo}}$ against V_G sensitivity, extracted from (e). The fitted $1/f$ noise (blue line) is above the setup-imposed dephasing limit (purple line), indicating additional on-chip noise.

second-excited state) suggests that E_J is dominated by two channels [38]. The tuning is repeatable upon small excursions (1–2 V), except for isolated deviations which we attribute to charge traps changing state. These changes—some are reproducible, others are stochastic—lead to jumps in f_{01}. Because the gatemon-resonator pair is well described by the dressed-state picture [1], f_{01} is easily found after a jump by measuring f_R and calculating f_{01}.

The strong V_G dependence of gatemon dephasing times allows a quantitative study of the effect of charge noise. Figure 3(e) clearly shows the presence of charge sweet spots, where the sensitivity $\partial f_{01}/\partial V_G$ vanishes and the dephasing times correspondingly peak. The ratio $T_\varphi^{\mathrm{Echo}}/T_\varphi^* \sim 8$ observed on and off the sweet spots (data not shown) indicates that the dominant dephasing noise is $1/f$ like [48]. From a linear fit of $\Gamma_\varphi^{\mathrm{Echo}}$ against $|\partial f_{01}/\partial V_G|$ [38,48–50], we extract a voltage-noise-independent offset of 66 ms^{-1} and a $1/f$ voltage noise amplitude $\sqrt{A_V} = 26\ \mu$V, where $S_{V,1/f} = A_V/|f|$. The extracted noise clearly exceeds the noise floor of the biasing circuit [38], indicating that on-chip charge noise dominates over electrical noise on the gate.

Now, we apply a $B_\parallel$ to the same gatemon. We focus on the gatemon because flux-tunable devices experience fluctuating f_{01} due to imperfect alignment and limited stability of $B_\parallel$. To disentangle $B_\parallel$ and V_G contributions, the gatemon is placed at the same V_G sweet spot for each $B_\parallel$ value. We attribute the observed monotonic decrease in f_{01} with $B_\parallel$ [Fig. 4(a)] to a reduced superconducting gap induced in the nanowire junction, $\Delta(B_\parallel) = \Delta(0)\sqrt{1-(B_\parallel/B_c)^2}$ [54]. The bulk of the CQED chip exhibits little change due to the high parallel critical field (B_c) of the NbTiN film [38,55]. We approximate the Andreev bound state energy with $V_i(\phi_i, B_\parallel) = -\Delta(B_\parallel)\sqrt{1-T_i\sin^2(\phi_i/2)}$. The Hamiltonian $\hat{H} = 4E_C\hat{N}^2 + V_A(\hat{\delta}, B_\parallel) + V_B(\hat{\delta}, B_\parallel)$ is fitted to f_{01} and $f_{02}/2$, fixing $\Delta(0)$ to the bulk Al gap and E_C to the value

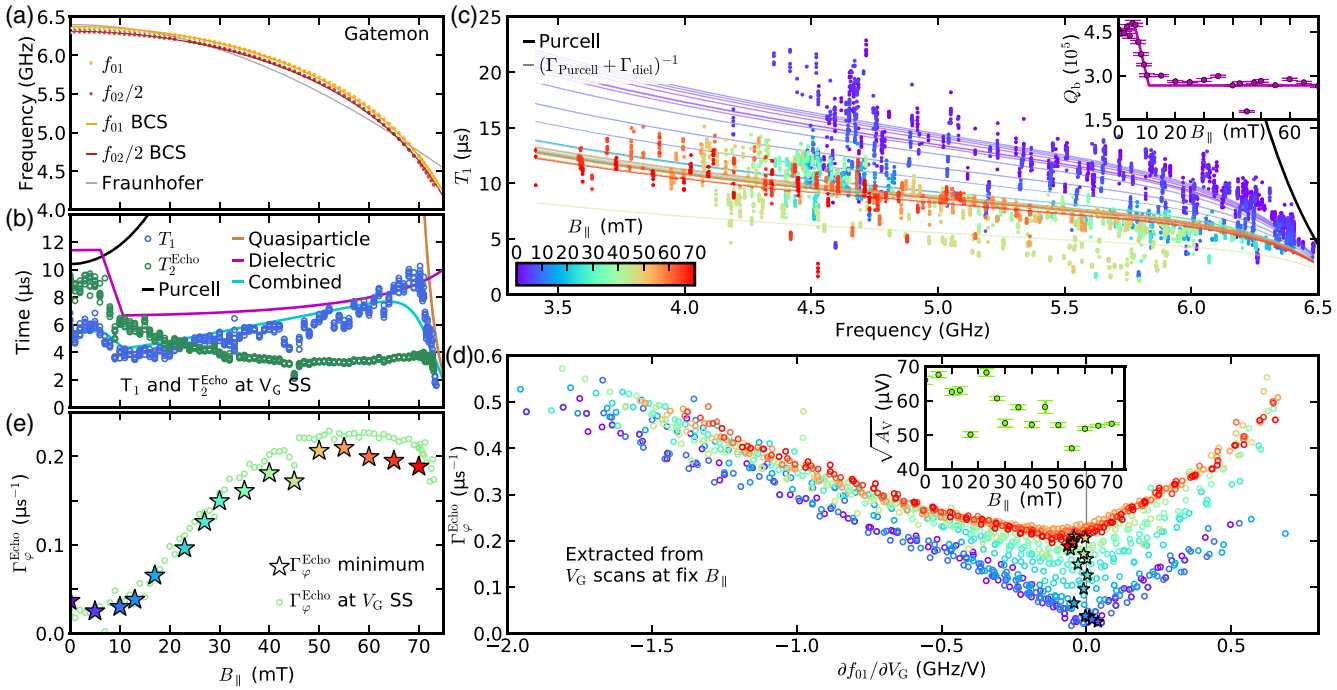

FIG. 4. Evolution of the gatemon of Fig. 3 in $B_\parallel$. (a) Qubit f_{01} and $f_{02}/2$ (orange and red dots) are described by a closing BCS gap (curves) with $B_c = 83.9$ mT. (b) At each value of $B_\parallel$, the gatemon is tuned to a V_G sweet spot (SS) to measure T_1 and T_2^{Echo} (blue and green symbols). At low $B_\parallel$ (f_{01} near the resonator), T_1 is mainly Purcell limited (red line). At $B_\parallel$ close to B_c the superconducting gap becomes so weak that quasiparticle tunneling dominates T_1 (brown, assumes 100 mK effective quasiparticle temperature). In between, the T_1 evolution can be attributed to a step in Q_b, see below. (c) T_1 versus frequency at different $B_\parallel$. Accounting for $T_1{}^P$, we fit a Q_b at each $B_\parallel$ (inset), finding a steplike drop from 6 to 10 mT. (d) Keeping $B_\parallel$ fixed [same color scale as (c)], V_G scans are performed to extract $\Gamma_\varphi^{\mathrm{Echo}}$, similar to Fig. 3(e). Inset: averaged extracted $1/f$ voltage noise amplitude. (e) Pure dephasing rates at V_G sweet spots versus $B_\parallel$ from data in (b) and (d). Stars are the interpolated minimal dephasing rates from (d).

obtained for the split-junction device. The best-fit parameters $T_{A,B} = 0.95$, 0.62 and $B_c = 83.9$ mT match f_{01} and $f_{02}/2$ with an average of the absolute residuals of 12.6 MHz. The extracted B_c of the Al shell is similar to other measurements of wires from this growth batch [34]. Because $B_\parallel$ is not collinear with the nanowires, the B_c of different qubits varies between 50 and 90 mT, roughly correlating with the nanowire-to-$B_\parallel$ alignment [38]. The B_c values stay constant during one cooldown and vary by ~5% between cooldowns, provided the sample orientation is kept fixed. Explaining the data by flux penetration of an extended junction (Fraunhofer model) [54] provides neither qualitative nor quantitative agreement.

Finally, we investigate the gatemon coherence properties in $B_\parallel$. At each $B_\parallel$ value, we extract T_1 and T_2^{Echo} [Fig. 4(b)] in a V_G sweep through a sweet spot. Before quasiparticle tunneling [53] dominates T_1 at 70 mT, we find a good match with a model including the Purcell effect [56] and a background field-dependent quality factor Q_b: $1/T_1(f_{01}, B_\parallel) = 1/T_1{}^{\mathrm{P}}(f_{01}) + 2\pi f_{01}/Q_b(B_\parallel)$. Here, Q_b decreases from 4.6×10^5 at $B_\parallel < 6$ mT to 2.7×10^5 at $B_\parallel > 10$ mT, as shown in the Fig. 4(c) inset. A similar steplike trend is observed in the internal quality factors of most resonators [38]. We surmise that the drop in Q_b is due to the Al wire bonds turning normal. Future experiments will use NbTiN air bridges to, hopefully, eliminate the effect. The dip in T_1 at 45 mT is reproducible but hysteretic. We do not understand its origin.

The field dependence of qubit dephasing is comparatively less understood. Tracking the V_G sweet spot, we observe that T_2^{Echo} is not T_1 limited above 20 mT [Fig. 4(b)]. The corresponding increase in $\Gamma_\varphi^{\mathrm{Echo}}$ [Fig. 4(e)] is reproduced when repeating the procedure of Fig. 3(f) at various $B_\parallel$ [Fig. 4(d)]. The gradual decrease in $\sqrt{A_V}$ and the shift of the minimum of $\Gamma_\varphi^{\mathrm{Echo}}$ away from $\partial f_{01}/\partial V_G = 0$ with $B_\parallel$ are also not understood. One possible explanation for these three effects may be that the sensitivity to the dominant on-chip charge noise differs from $\partial f_{01}/\partial V_G$ away from $B_\parallel = 0$ around the one sweet spot that we tracked. Studying the dephasing around multiple V_G sweet spots (not possible with this gatemon and cooldown) may allow us to test this hypothesis in the future.

In summary, first, we have characterized flux- and gate-tunable nanowire transmons with state-of-the-art T_1 at $B_\parallel = 0$, focusing on quantitative extraction of flux and charge noise coupling to the Josephson energy. Next, we

have investigated the evolution of a gatemon in $B_\parallel$ up to 70 mT, the upper bound set by the closing of the induced gap. Several features of the T_1 and T_2^{Echo} dependence in $B_\parallel$ are not understood yet, inviting further theoretical and experimental investigation.

Our immediate next experiments will further the study and development of nanowire transmons in a magnetic field. Using a persistent current mode for the solenoid providing $B_\parallel$, we aim to investigate the spectrum and coherence of flux-tunable transmons in $B_\parallel$. This could yield further insight into the microscopic origin of $1/f$ flux noise [52]. Studying the temperature and $B_\parallel$ behavior of the observed charge traps may lead to further understanding of their nature. Nanowires with a thinner, partial shell (10 nm), which have already been shown to induce a hard superconducting gap [57], will allow operation of nanowire transmons up to 0.5 T, reaching the relevant field range for attractive new applications of CQED.

We thank A. Akhmerov, A. Geresdi, G. de Lange, and M. de Moor for discussions, D. Thoen for depositing the NbTiN film, and R. Schouten and J. Watson for technical assistance. We acknowledge funding by Microsoft Corporation Station Q, the Dutch organization for Fundamental Research on Matter (FOM), the Netherlands Organization for Scientific Research via the Frontiers of Nanoscience program (NWO)/Dutch Ministry of Education, Culture and Research (OCW), an European Research Council (ERC) Synergy grant, and the Danish National Research Foundation.

*Corresponding author.
l.dicarlo@tudelft.nl

[1] A. Blais, R.-S. Huang, A. Wallraff, S. M. Girvin, and R. J. Schoelkopf, Phys. Rev. A **69**, 062320 (2004).
[2] A. Wallraff, D. I. Schuster, A. Blais, L. Frunzio, R.-S. Huang, J. Majer, S. Kumar, S. M. Girvin, and R. J. Schoelkopf, Nature (London) **431**, 162 (2004).
[3] B. D. Josephson, Phys. Lett. **1**, 251 (1962).
[4] Y. Nakamura, Y. Pashkin, and J. Tsai, Nature (London) **398**, 786 (1999).
[5] R. Barends *et al.*, Nature (London) **508**, 500 (2014).
[6] L. Steffen, Y. Salathe, M. Oppliger, P. Kurpiers, M. Baur, C. Lang, C. Eichler, G. Puebla-Hellmann, A. Fedorov, and A. Wallraff, Nature (London) **500**, 319 (2013).
[7] M. Jerger, Y. Reshitnyk, M. Oppliger, A. Potočnik, M. Mondal, A. Wallraff, K. Goodenough, S. Wehner, K. Juliusson, N. K. Langford, and A. Fedorov, Nat. Commun. **7**, 12930 (2016).
[8] D. Ristè, M. Dukalski, C. A. Watson, G. de Lange, M. J. Tiggelman, Y. M. Blanter, K. W. Lehnert, R. N. Schouten, and L. DiCarlo, Nature (London) **502**, 350 (2013).
[9] E. P. Harris and D. Mapother, Phys. Rev. **165**, 522 (1968).
[10] A. Imamoglu, Phys. Rev. Lett. **102**, 083602 (2009).
[11] T. Hyart, B. van Heck, I. C. Fulga, M. Burrello, A. R. Akhmerov, and C. W. J. Beenakker, Phys. Rev. B **88**, 035121 (2013).
[12] V. Mourik, K. Zuo, S. M. Frolov, S. R. Plissard, E. P. a. M. Bakkers, and L. P. Kouwenhoven, Science **336**, 1003 (2012).
[13] J. M. Kosterlitz and D. J. Thouless, J. Phys. C **6**, 1181 (1973).
[14] A. Andreev, J. Exp. Theor. Phys. **19**, 1228 (1964).
[15] J. Pillet, C. Quay, P. Morfin, C. Bena, A. L. Yeyati, and P. Joyez, Nat. Phys. **6**, 965 (2010).
[16] D. J. van Woerkom, A. Proutski, B. van Heck, D. Bouman, J. I. Väyrynen, L. I. Glazman, P. Krogstrup, J. Nygård, L. P. Kouwenhoven, and A. Geresdi, Nat. Phys. **13**, 876 (2017).
[17] T. Yokoyama, M. Eto, and Y. V. Nazarov, J. Phys. Soc. Jpn. **82**, 054703 (2013).
[18] N. Samkharadze, A. Bruno, P. Scarlino, G. Zheng, D. P. DiVincenzo, L. DiCarlo, and L. M. K. Vandersypen, Phys. Rev. Applied **5**, 044004 (2016).
[19] M. Popinciuc, V. E. Calado, X. L. Liu, A. R. Akhmerov, T. M. Klapwijk, and L. M. K. Vandersypen, Phys. Rev. B **85**, 205404 (2012).
[20] Y.-J. Doh, J. A. van Dam, A. L. Roest, E. P. Bakkers, L. P. Kouwenhoven, and S. De Franceschi, Science **309**, 272 (2005).
[21] E. Pallecchi, M. Gaaß, D. Ryndyk, and C. Strunk, Appl. Phys. Lett. **93**, 072501 (2008).
[22] M. L. Della Rocca, M. Chauvin, B. Huard, H. Pothier, D. Esteve, and C. Urbina, Phys. Rev. Lett. **99**, 127005 (2007).
[23] C. Janvier, L. Tosi, L. Bretheau, Ç. Girit, M. Stern, P. Bertet, P. Joyez, D. Vion, D. Esteve, M. Goffman, H. Pothier, and C. Urbina, Science **349**, 1199 (2015).
[24] G. de Lange, B. van Heck, A. Bruno, D. J. van Woerkom, A. Geresdi, S. R. Plissard, E. P. A. M. Bakkers, A. R. Akhmerov, and L. DiCarlo, Phys. Rev. Lett. **115**, 127002 (2015).
[25] T. W. Larsen, K. D. Petersson, F. Kuemmeth, T. S. Jespersen, P. Krogstrup, J. Nygård, and C. M. Marcus, Phys. Rev. Lett. **115**, 127001 (2015).
[26] L. Casparis, T. W. Larsen, M. S. Olsen, F. Kuemmeth, P. Krogstrup, J. Nygård, K. D. Petersson, and C. M. Marcus, Phys. Rev. Lett. **116**, 150505 (2016).
[27] S. Chuang, Q. Gao, R. Kapadia, A. C. Ford, J. Guo, and A. Javey, Nano Lett. **13**, 555 (2013).
[28] Y.-Y. Liu, J. Stehlik, C. Eichler, M. Gullans, J. M. Taylor, and J. Petta, Science **347**, 285 (2015).
[29] J. Koch, T. M. Yu, J. Gambetta, A. A. Houck, D. I. Schuster, J. Majer, A. Blais, M. H. Devoret, S. M. Girvin, and R. J. Schoelkopf, Phys. Rev. A **76**, 042319 (2007).
[30] D. J. Thoen, B. G. C. Bos, E. Haalebos, T. Klapwijk, J. Baselmans, and A. Endo, IEEE Trans. Appl. Supercond. **27**, 1 (2017).
[31] B. G. C. Bos, D. J. Thoen, E. Haalebos, P. Gimbel, T. Klapwijk, J. Baselmans, and A. Endo, IEEE Trans. Appl. Supercond. **27**, 1 (2017).
[32] A. Bruno, G. de Lange, S. Asaad, K. L. van der Enden, N. K. Langford, and L. DiCarlo, Appl. Phys. Lett. **106**, 182601 (2015).
[33] P. Krogstrup, N. L. B. Ziino, W. Chang, S. M. Albrecht, M. H. Madsen, E. Johnson, J. Nygård, C. M. Marcus, and T. S. Jespersen, Nat. Mater. **14**, 400 (2015).
[34] W. Chang, S. M. Albrecht, T. S. Jespersen, F. Kuemmeth, P. Krogstrup, J. Nygård, and C. M. Marcus, Nat. Nanotechnol. **10**, 232 (2015).

[35] C. Wang, Y. Y. Gao, I. M. Pop, U. Vool, C. Axline, T. Brecht, R. W. Heeres, L. Frunzio, M. H. Devoret, G. Catelani, L. I. Glazman, and R. J. Schoelkopf, Nat. Commun. **5**, 5836 (2014).
[36] Ö. Gül, D. J. Van Woerkom, I. van Weperen, D. Car, S. R. Plissard, E. P. Bakkers, and L. P. Kouwenhoven, Nanotechnology **26**, 215202 (2015).
[37] J. M. Martinis, M. Ansmann, and J. Aumentado, Phys. Rev. Lett. **103**, 097002 (2009).
[38] See Supplementarl Material at http://link.aps.org/supplemental/10.1103/PhysRevLett.120.100502 for details on the experimental setup, the fabrication procedure, the image recognition software, the frequency splitting of a gatemon, the PSD of the investigated TLS, the number of channels contributing to the Josephson energy, coherence limitations, voltage noise, magnetic field noise and the performance of resonators in a magnetic field..
[39] Itseez, Open source computer vision library, https://github.com/itseez/opencv.
[40] N. Otsu, IEEE Trans. Syst. Man Cybern. **9**, 62 (1979).
[41] J. Serra, *Image Analysis & Mathematical Morphology* (Academic Press, New York, 1997).
[42] J. Canny, IEEE Trans. Pattern Anal. Mach. Intell. **PAMI-8**, 679 (1986).
[43] D. H. Ballard, Pattern Recognit. **13**, 111 (1981).
[44] F. Motzoi, J. M. Gambetta, P. Rebentrost, and F. K. Wilhelm, Phys. Rev. Lett. **103**, 110501 (2009).
[45] R. Barends, J. Wenner, M. Lenander, Y. Chen, R. C. Bialczak, J. Kelly, E. Lucero, P. O'Malley, M. Mariantoni, D. Sank, H. Wang, T. C. White, Y. Yin, J. Zhao, A. N. Cleland, J. M. Martinis, and J. J. A. Baselmans, Appl. Phys. Lett. **99**, 113507 (2011).
[46] S. Asaad, C. Dickel, S. Poletto, A. Bruno, N. K. Langford, M. A. Rol, D. Deurloo, and L. DiCarlo, npj Quantum Inf. **2**, 16029 (2016).
[47] M. Jerger, S. Poletto, P. Macha, U. Hübner, E. Il'ichev, and A. V. Ustinov, Appl. Phys. Lett. **101**, 042604 (2012).
[48] J. M. Martinis, S. Nam, J. Aumentado, K. M. Lang, and C. Urbina, Phys. Rev. B **67**, 094510 (2003).
[49] F. Yoshihara, K. Harrabi, A. O. Niskanen, Y. Nakamura, and J. S. Tsai, Phys. Rev. Lett. **97**, 167001 (2006).
[50] M. D. Hutchings, J. B. Hertzberg, Y. Liu, N. T. Bronn, G. A. Keefe, M. Brink, J. M. Chow, and B. L. T. Plourde, Phys. Rev. Applied **8**, 044003 (2017).
[51] P. Kumar, S. Sendelbach, M. A. Beck, J. W. Freeland, Z. Wang, H. Wang, C. C. Yu, R. Q. Wu, D. P. Pappas, and R. McDermott, Phys. Rev. Applied **6**, 041001 (2016).
[52] W. D. Oliver and P. B. Welander, MRS Bull. **38**, 816 (2013).
[53] D. Ristè, C. C. Bultink, M. J. Tiggelman, R. N. Schouten, K. W. Lehnert, and L. DiCarlo, Nat. Commun. **4**, 1913 (2013).
[54] M. Tinkham, *Introduction to Superconductivity*, 2nd ed. (McGraw-Hill, New York, 1996).
[55] D. Bothner, T. Gaber, M. Kemmler, D. Koelle, R. Kleiner, S. Wünsch, and M. Siegel, Phys. Rev. B **86**, 014517 (2012).
[56] A. A. Houck, J. A. Schreier, B. R. Johnson, J. M. Chow, J. Koch, J. M. Gambetta, D. I. Schuster, L. Frunzio, M. H. Devoret, S. M. Girvin, and R. J. Schoelkopf, Phys. Rev. Lett. **101**, 080502 (2008).
[57] S. Gazibegovic, D. Car, H. Zhang, S. C. Balk, J. A. Logan, M. W. de Moor, M. C. Cassidy, R. Schmits, D. Xu, G. Wang, P. Krogstrup *et al.*, Nature (London) **548**, 434 (2017).